JOURNAL OF Materials CHEMISTRY

Cobalt substitution in lithium manganate spinels: examination of local structure and lithium extraction by XAFS

Phillip Aitchison,[a,b] Brett Ammundsen,[a] Deborah J. Jones,*[a] Gary Burns[b] and Jacques Rozière[a]

[a]*Laboratoire des Agrégats Moléculaires et Matériaux Inorganiques ESA CNRS 5072, Université Montpellier 2, 34095 Montpellier, CEDEX 5, France*
[b]*School of Chemistry and Physics, Victoria University of Wellington, New Zealand*

Received 19th July 1999, Accepted 24th September 1999

Lithium manganate spinel $LiMn_2O_4$ was partially substituted with Co and chemically delithiated and relithiated. Variations in the local structure surrounding the substitutional ion, which are probed by EXAFS and XANES, are related to the long range (average) structure and performance as battery cathode materials. The substituent ion is randomly distributed in the spinel and present as trivalent ions replacing Mn^{3+}. The substituent ion stabilises the lattice through a reduction in Jahn–Teller distortion of the lattice at the local level, but can limit the quantity of lithium that may be extracted due to its redox inactivity at potentials up to *ca.* 4 V. The 5 V plateau reported during the electrochemical extraction of Li from $LiCo_xMn_{2-x}O_4$ appears to be due to oxidation of Co^{3+} to Co^{4+}.

Introduction

Lithium manganese oxides having the spinel structure have the potential to reduce considerably the economic cost and environmental impact of advanced rechargeable batteries. These spinels are particularly versatile in terms of modification of their stoichiometries to give properties tailored to specific tasks; most notably they can incorporate large amounts of substitutional ions and changes in lithium and oxygen stoichiometry while retaining the spinel crystal structure.

Many recent studies have examined the changes that occur in the bulk structure of cation substituted $LiMn_2O_4$ spinel, and properties that arise from such structural modification.[1–7] However, ionic substitution induces *local* structural and electronic perturbations, which can affect lithium diffusion in the lattice and so their chemical and electrochemical performance. Understanding the effect of cation substitution on the local structure of the lithium manganate spinels provides important insights into how the structure of these materials can be tailored to give optimum chemical and electronic properties.

Several electrochemical studies have attempted to improve the performance of $LiMn_2O_4$ as a 4 V battery cathode by partially substituting Mn with trivalent cations such as Co,[1] Cr[2] and Ni.[3] Substitution was found to decrease the capacity of the cell by reducing the quantity of oxidisable Mn^{3+} and replacing it with, under the conditions used, a non-oxidisable cation.[4] The improvements in cyclability that are observed when Mn^{3+} is substituted by other cations can be attributed to an increase in lattice stability given by a reduction in the local distortion of the lattice by Jahn–Teller (JT) stabilised Mn^{3+}. In $LiMn_2O_4$, where the average manganese oxidation state is $+3.5$ and the locally distorted $Mn^{III}O_6$ octahedra are randomly orientated, the JT stabilisation remains anisotropic above 280 K.[8] However, it is thought that in battery cathodes repeated cycling of manganese between the oxidation states of $+3$ and $+4$ leads to structural disruption that can reduce the cyclability of lithium extraction, giving diminished rechargeability in lithium batteries. Partial substitution of manganese by other cations, such as Co, Cr, Ga and Ti,[6] can be used to tailor the properties of $LiMn_2O_4$ both to improve the cycling and change the electrochemical behaviour of rechargeable battery cathodes.

Recent improvements in electrolyte technology have made it possible to explore the potential range of electrochemical cells to over 5 V *versus* a lithium metal anode. A recent study has reported reversible lithium extraction at *ca.* 5.1 V in $LiMn_2O_4$ partially substituted by cobalt.[6] Although the mechanism responsible for this high potential lithium extraction/insertion was not explained, the possibility of high voltage (>5 V), reversible lithium battery cathodes is extremely interesting.

A better understanding of the structural effects of transition-metal substituents can be gained by examining the local structural and electronic environment of the substituted cation (M). Our recent X-ray Absorption Spectroscopy (XAS) investigation of chromium substituted $LiMn_2O_4$ examined the stabilisation of the short range structure that occurs when Cr^{3+} is substituted for Mn^{3+}.[7] The reversible chemical extraction and re-insertion of lithium takes place with changes in the oxidation state of the Mn, while chromium remains stable as a trivalent species. The replacement of the Jahn–Teller distorted Mn^{3+} cation by Cr^{3+} reduces local disorder in the lattice.

The close similarity in size between Co^{3+} and Mn^{4+}, its high octahedral stabilisation energy and the possibility of oxidation makes cobalt an attractive substituent in the spinel lithium manganates. Observation of changes in the short, medium and long range structure of $LiCo_xMn_{2-x}O_4$ ($0 \leqslant x \leqslant 1$) by XAS and X-Ray Diffraction (XRD), coupled with chemical analyses, allow the effects of substituting cobalt for manganese to be observed and explained.

Experimental

Lithium manganate spinels of the formula $LiCo_xMn_{2-x}O_4$ ($0 \leqslant x \leqslant 1$) were prepared from $MnCO_3$ (Aldrich, 99.9+%), $CoC_2O_4{\cdot}xH_2O$ (Aldrich) and Li_2CO_3 (Aldrich, 99.997%). The powders were ground, heated in air to 750 °C in three 24 hour cycles with grinding between each cycle, followed by cooling at 2 °C min^{-1} to room temperature. Delithiation and relithiation were carried out by stirring in 0.5 M HCl and 0.1 M LiOH respectively, followed by washing with distilled water and drying at room temperature in air.

Powder X-ray diffraction patterns were recorded using Cu-

Kα radiation on an automated Philips diffractometer and analysed using the Rietveld program FullProf.[9] Chemical compositions were determined from atomic analysis by flame spectrometry. Combined oxidation states of manganese and cobalt were determined by a standard technique of reduction with sodium oxalate and titration of the excess with potassium permanganate solution.[10] Analyses were performed in triplicate, with an uncertainty of ±2%. For the purpose of manganese oxidation state calculation, cobalt was assumed to be trivalent, an assumption justified by XAFS data presented below.

X-Ray absorption spectra at the Mn and Co K edges were obtained at *ca.* 77 K in transmission mode on the EXAFS 13 spectrometer at the 1.85 GeV, 300 mA synchrotron source, la Laboratoire pour l'Utilisation du Rayonnement Électromagnetique (LURE), France. X-Ray Absorption Near Edge Structure (XANES) spectra were obtained in 0.3 eV steps using a detuned Si[311] double diffraction monochromator. Extended X-Ray Absorption Fine Structure (EXAFS) spectra were measured using a Si[111] monochromator in 3 eV steps to approximately 1000 eV after the edge. Energy calibration was carried out for all measurements by the appropriate metal foil placed after the I_1 ion chamber detector. Samples were prepared as fine dispersions in boron nitride/Nujol mulls contained between Parafilm windows; concentrations were optimised to give an edge jump of one.

XAFS data were analysed using the programs of Michalowicz.[11] Background subtraction was by linear extrapolation of the pre-edge and EXAFS spectra were individually normalised in the $\mu_{0,\mathrm{exp}}-\mu_{1,\mathrm{exp}}$ convention, simulating $\mu_{0,\mathrm{exp}}$ with third order spline functions. Fourier transforms were performed on averaged EXAFS spectra (3 scans) with k^3 weighting of a Kaiser window ($\tau=3.5$), followed by curve fitting of the Fourier filtered EXAFS spectra using *ab initio* phase (φ), amplitude (A) and mean free path (λ) functions calculated for spinel LiM_2O_4 by Feff 7.0,[12] where M was Mn or Co as appropriate. Refining the bond distances of model compounds using these functions gave close agreement with the expected results. Multiple scattering effects were determined to be not significant to EXAFS derived structural parameters for the first two atom shells after theoretical modelling with Feff, which was confirmed during the data fitting process.

Results and discussion

I. $LiCo_xMn_{2-x}O_4$

The experimentally determined chemical compositions and cell parameters for the $LiCo_xMn_{2-x}O_4$ ($0\leqslant x\leqslant 1$) compounds are given in Table 1. Powder X-ray diffraction data show that substitution of cobalt into $LiMn_2O_4$ does not change the *Fd*3*m* space group symmetry. Low spin Co^{3+} has an ionic radius of 0.55 Å, compared with 0.65 and 0.53 Å for Mn^{3+} and Mn^{4+} respectively. A contraction of the unit cell was observed with increasing amounts of cobalt, consistent with replacement of Mn^{3+} with Co^{3+}.

Addition of cobalt improves the crystallinity of the spinel, giving markedly narrower XRD peak widths and larger crystallite sizes as observed by scanning electron microscopy. This increase in crystallinity is observed for cobalt doped spinels prepared at temperatures as low as 400 °C, as can be seen in Fig. 1. As the quantity of cobalt is increased, changes in the intensity ratio of the [311] and [400] reflections indicate the presence of heavy cations in the 8a tetrahedral site, although the [220] peak, which is sensitive to the presence of heavy cations in the 8a site, is only observed weakly. Rietveld refinement calculations show that the changes in the XRD patterns may correspond to a small quantity of transition metal in the 8a site, to a maximum of 5% in the end member $LiCoMnO_4$. Both Mn^{3+} and Mn^{4+} are energetically more stable in octahedral co-ordination, as is Co^{3+}, so the most likely 8a-site tetrahedral cation is residual unoxidised Co^{2+}.

X-Ray absorption spectra at the Co and Mn K edges (XANES) are shown in Fig. 2 and 3. We have already shown that the position of the Mn absorption edge depends on the manganese oxidation state ($+3\leqslant OS_{\mathrm{Mn}}\leqslant +4$) in spinels,[13] and Fig. 2 clearly shows that there is a large difference in the edge

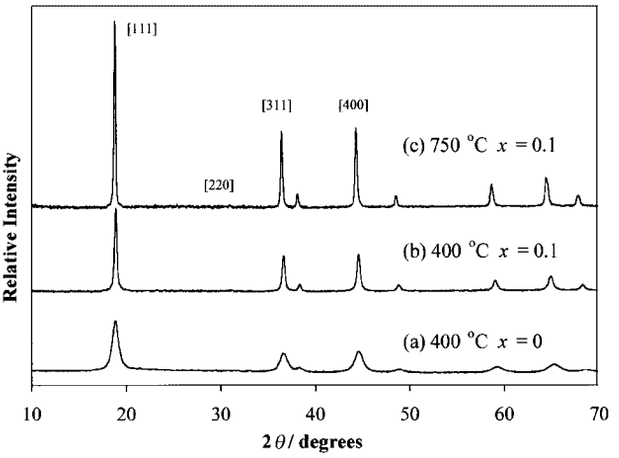

Fig. 1 Powder XRD patterns of (a) $LiMn_2O_4$ (400 °C), (b) $LiCo_{0.1}Mn_{1.9}O_4$ (400 °C) and (c) $LiCo_{0.1}Mn_{1.9}O_4$ (750 °C).

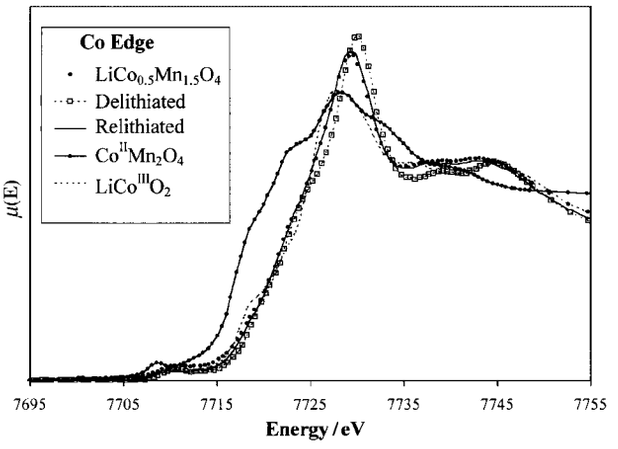

Fig. 2 XANES at the cobalt K edge of $LiCo_xMn_{2-x}O_4$, where the spectra are identical for $x=0.1$, 0.2 or 0.5, and for comparison $CoMn_2O_4$ and $LiCoO_2$.

Table 1 Chemical composition and cell parameters of spinel $LiCo_xMn_{2-x}O_4$

x	Chemical composition	Co + Mn mean oxidation state	Cell parameter a_0/Å
0	$(Li_{0.96})[Mn^{III}_{1.04}Mn^{IV}_{0.98}]O_4$	3.48	8.239(1)
0.1	$(Li_{1.00})[Co_{0.10}Mn^{III}_{0.82}Mn^{IV}_{1.06}]O_4$	3.53	8.212(1)
0.2	$(Li_{1.01})[Co_{0.20}Mn^{III}_{0.69}Mn^{IV}_{1.07}]O_4$	3.54	8.191(5)
0.5	$(Li_{0.99})[Co_{0.51}Mn^{III}_{0.47}Mn^{IV}_{1.02}]O_4$	3.57	8.127(3)
1	$(Li_{0.97})[Co_{0.97}Mn^{IV}_{1.03}]O_4$	3.52	8.061(1)

[a]Assumes all cobalt is trivalent. ( ) and [ ] denote tetrahedral and octahedral site occupancy, respectively.

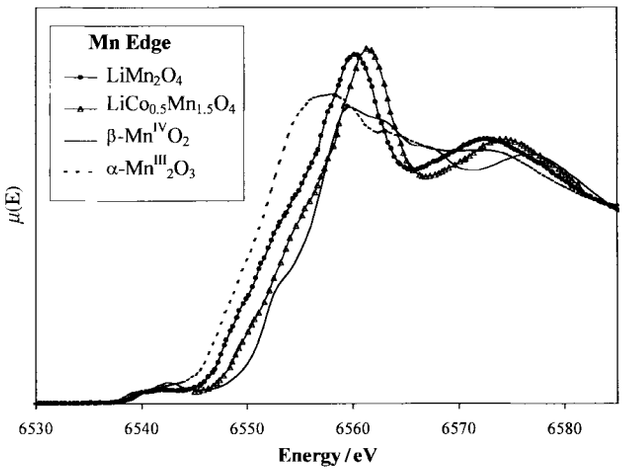

Fig. 3 XANES at the manganese K edge of $LiMn_2O_4$, $LiCo_{0.5}Mn_{1.5}O_4$, β-MnO_2 and α-Mn_2O_3, showing the edge shift with increasing manganese oxidation state.

position between tetrahedral Co^{2+} in $CoMn_2O_4$ and the octahedral Co^{3+} of $LiCoO_2$. The XANES spectra at the cobalt edge of the substituted manganese spinels are identical to one another and the edge is observed at the same energy as that of $LiCoO_2$. This, and the similarity in the shape of the XANES at the Co and Mn edges of the spinel, strongly support cobalt as being predominantly trivalent and present in 16d octahedral sites. This agrees with reported electron energy loss spectra of Co substituted $LiMn_2O_4$.[14] XANES at the manganese K edge in Fig. 3 illustrates the shift in the edge position corresponding to an increasing average Mn oxidation state. The magnitudes of the shifts are consistent with the chemically determined oxidation states given in Table 1.

Fourier transforms of the EXAFS spectra and examples of the quality of fit at the cobalt and manganese edges are given in Fig. 4 and 5. Phase corrections have not been applied to the FT spectra presented, so the peaks are shifted by approximately −0.4 Å. Maxima at *ca.* 1.5 and 2.5 Å are due to the first M–O and M–M co-ordination shells respectively. Fourier filtered over the range *ca.* $R=1$ to 3 Å, the *k*-space data (Fig. 4b and 5b) could be fully accounted for by two contributions to the EXAFS, one shell of six-co-ordinate M–O at *ca.* 1.9 Å and one of six co-ordinate M–M at *ca.* 2.9 Å, in accordance with established crystallographic data on $LiMn_2O_4$.[15] At low *k* (<3 Å^{-1}) multiple scattering contributions become more important, causing some deviation from the fit, which uses a single scattering formulation. However, the refined interatomic distances and Debye–Waller factors determined for each sample, and given in Table 2, do not change significantly with the inclusion of multiple scattering.

Substituting Co^{3+} for Mn^{3+} in $LiMn_2O_4$ produces a shortening of the average Mn–O bond length with increasing cobalt substitution. A decrease in the Debye–Waller factor (σ) is also observed, consistent with an increase in the symmetry of the average Mn environment caused by the reduction in the number of Mn^{3+} ions. A slight increase in the Co–O bond distance (R_{Co-O}) and of σ is observed for $LiCoMnO_4$. This goes against the trend of cobalt substitution up to $x=0.5$, which may be due to the presence of a small quantity of Co^{2+}, as is suggested by the above XRD data.

A difference is observed between the manganese–metal (R_{Mn-M}) and cobalt–metal (R_{Co-M}) bond lengths (M = Co or Mn). This is not seen by XRD which averages the local Co and Mn environments to give the long range structure. Substituting Mn^{3+} with the smaller non-JT Co^{3+} reduces lattice strain about the substituted 16d site, and the shorter Co–M distance observed by XAFS shows that the manganese lattice contracts about cobalt. This local contraction and the difference in

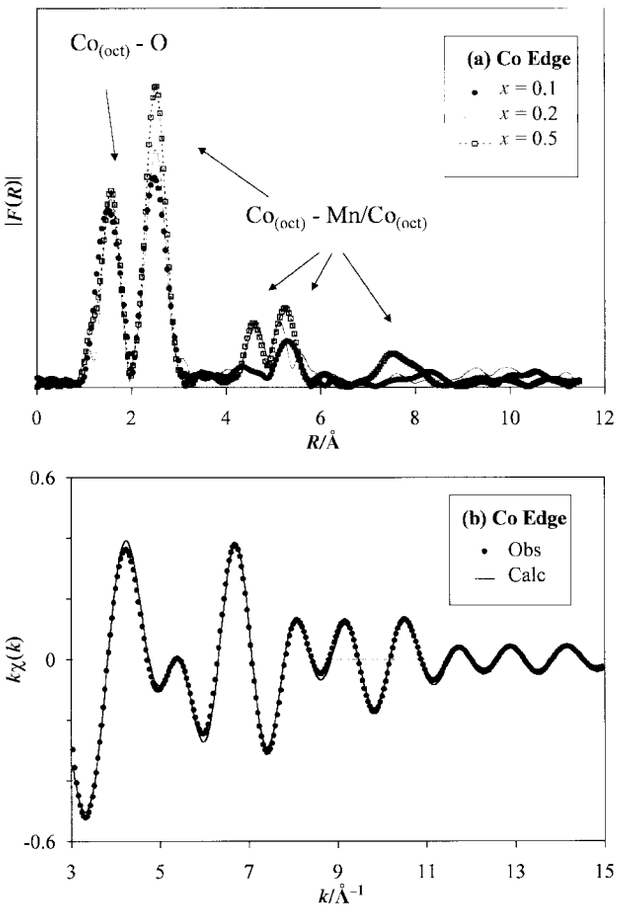

Fig. 4 (a) Fourier transforms of the cobalt edge EXAFS of $LiCo_xMn_{2-x}O_4$ for $x=0.1$, 0.2 or 0.5 illustrating the increasing influence of back scattering from the Co–M pair as *x* increases. (b) *k*-Space data for $x=0.5$ and curve fit.

Coulombic repulsion between Co^{3+}/Mn^{4+} and Mn^{4+}/Mn^{4+} means that the average Co–M bond length is shorter than that observed for Mn–M. The difference between R_{Mn-M} and R_{Co-M} decreases as the cobalt content is increased (Table 2). In the long range structure an increasing number of Co–M interactions appears as a continuous decrease in the cell parameter, from 8.24 Å in $LiMn_2O_4$ to 8.07 Å in $LiCoMnO_4$. In the case of chromium substitution of $LiMn_2O_4$,[7] the close similarity in size between Cr^{3+} and Mn^{3+} means that this contraction about the dopant is not observed to the same extent.

Attempts were made to distinguish between shells of manganese and cobalt back-scatterers in the local environment. Feff generated phase and amplitude functions for these compounds have previously been shown to be as good as, or better than, other estimations of these functions for spinel lithium manganates.[13] Although comparison of the theoretical phase and amplitude functions for back-scattering by manganese and cobalt shows a distinct difference, in practice it was only possible to make this distinction for the phases richest in cobalt, $LiCo_xMn_{2-x}O_4$, where $x\geqslant0.5$. Here, the first cation shell of $LiCo_{0.5}Mn_{1.5}O_4$ was allowed to refine as two separate sub-shells, one shell of cobalt neighbours and another of manganese. The occupancies of the two sub-shells were linked and fixed to a total of six. Refinement gave R_{Co-Mn} and R_{Co-Co} distances of 2.88(1) and 2.81(1) Å respectively. Occupancies of the sub-shells gave agreement with statistically distributed cobalt with no evidence for cobalt clustering. A similar splitting of the first cation shell could be fitted about manganese atoms. These results are in agreement with the observed local contraction about cobalt ions. However, in both cases using only one shell of back-scattering

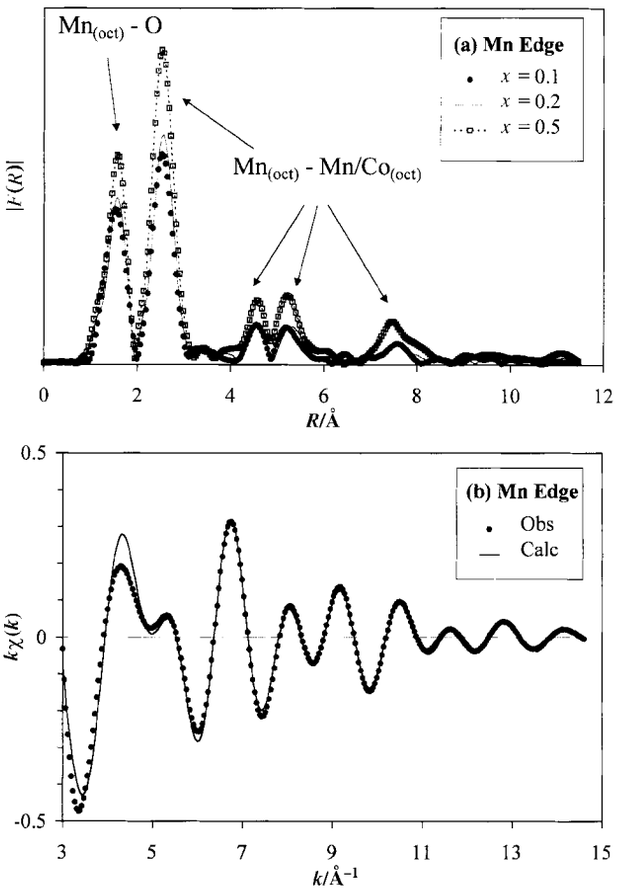

Fig. 5 (a) Fourier transforms of the manganese edge EXAFS of $LiCo_xMn_{2-x}O_4$ for $x=0.1$, 0.2 or 0.5 illustrating the increasing influence of the back scattering from both Mn–O and Mn–M pairs as x increases. (b) k-Space data for $x=0.5$ and curve fit.

manganese atoms gave a fit of almost identical quality to that obtained using separate shells of manganese and cobalt. Thus, despite the appeal of a model which corresponds to the chemical formulation of the spinel, the model used to fit the data presented in Table 2 treats cobalt back-scatterers as being equivalent to manganese, in accordance with the principle of Occam's Razor.[16] Thus, the model retained from a set giving equally satisfactory results is that which describes the system with the least number of adjustable parameters.

II. Lithium extraction and re-insertion

Extraction of lithium from lithium manganate spinels can be accomplished by: (i) disproportionation of Mn^{3+} to Mn^{4+} and water soluble Mn^{2+}, as proposed by Hunter;[17] (ii) lithium↔proton exchange,[18,19] or (iii) a combination of these two processes.[20,21]

Table 3 gives the chemical compositions and cell parameters of the chemically delithiated and relithiated cobalt doped spinels. Practically all (>90%) of the lithium may be extracted from the non-doped spinel ($x=0$), and as the quantity of substituted cobalt increases less lithium can be extracted. When lithium manganate spinels have an 'excess' of lithium which occupies some of the 16d sites, as in the $Li_{1+x}Mn_{2-x}O_4$ ($0<x\leqslant 0.33$) spinels, aqueous acid extracts the 16d lithium and inserts protons into the structure of the spinel.[22] Thermal analysis and infrared spectroscopy provide no evidence for proton insertion in the delithiated spinel $Li_yCo_xMn_{2-x}O_4$, as is expected from the chemical formulations given in Table 1. The mean oxidation state of the transition metals increases upon delithiation. Both the amount of residual lithium (y) and the mean oxidation state of the transition metal are approximately linear functions of the quantity of cobalt (x). Relithiation of $Li_yCo_xMn_{1-x}O_4$ appears to be limited to $y=ca.$ 0.90, regardless of the quantity of cobalt, with both oxidation state and cell parameter proportionally returning to that of the corresponding parent spinel. In $LiCoMnO_4$ ($x=1$) no lithium can be extracted under the conditions used here.

After delithiation or relithiation there is no longer indication from the XRD data of transition metal cations in 8a sites. This suggests that the inferred tetrahedral cobalt in the parent materials is indeed Co^{2+}, which is either dissolved out of the lattice during lithium extraction, or migrates into octahedral co-ordination as Co^{3+}.

XANES allows changes in the oxidation state of the transition metal ions on lithium extraction and insertion to be observed separately as the individual contributions of cobalt and manganese. No change can be observed in the XANES at the Co edge for the delithiated and relithiated spinels, indicating that there is little or no change in the cobalt oxidation state during lithium extraction or reinsertion. Energy shifts in XANES at the Mn edge shows that the changes in oxidation state determined by chemical analysis can be attributed entirely to the oxidation of manganese.

Structural parameters derived from EXAFS data for the $LiCo_{0.20}Mn_{1.80}O_4$ ($x=0.2$) delithiation and relithiation series are given as an example in Table 4. Fig. 6 and 7 show the changes that occur in the Fourier transform upon lithium extraction and reinsertion. Oxidation of manganese from Mn^{3+} to Mn^{4+} on delithiation is reflected in a shortening of the Mn–O bond length and a reduction in σ_{Mn-O}. A similar decrease is seen in R_{Mn-M} due to the reduction in cell volume and in σ_{Mn-M} due to the diminished localised Jahn–Teller distortion of the lattice. The changes observed in the EXAFS at the Mn edge for cobalt doped $LiMn_2O_4$ are in close qualitative agreement with those previously reported for non-doped $LiMn_2O_4$.[13]

Table 2 EXAFS determined structural parameters for spinel $LiCo_xMn_{2-x}O_4$

		M–O		M–M		
M	x	R^a/Å	σ/Å	R^a/Å	σ/Å	Residue (%)[b]
Mn	0	1.925	0.080	2.904	0.074	—
	0.1	1.913	0.078	2.899	0.077	2.3
	0.2	1.908	0.070	2.898	0.074	1.1
	0.5	1.907	0.057	2.876	0.063	2.6
	1	1.906	0.057	2.866	0.061	2.7
Co	0.1[c]	1.929	0.055	2.873	0.060	1.9
	0.2	1.929	0.056	2.877	0.067	2.8
	0.5	1.924	0.052	2.869	0.056	1.9
	1	1.937	0.057	2.872	0.060	3.4

[a]Uncertainties in distances (±0.01 Å) are estimated from the difference between EXAFS refined values and those obtained from X-ray diffraction in the reference compound $LiMn_2O_4$. [b]Residue $=\Sigma_k(k[\chi_{exp}(k)]-k[\chi_{calc}(k)])^2k^3/\Sigma_k(k[\chi_{exp}(k)]^2-k^3)$. [c]Cobalt edge data were collected in fluorescence mode for this sample.

Table 3 Chemical composition and cell parameters of delithiated and relithiated cobalt substituted lithium manganate spinels

$LiCo_xMn_{2-x}O_4$		Chemical composition[a]	Co+Mn mean oxidation state	Cell parameter, a_0/Å
$x=0$	Delith.	$(Li_{0.11})[Mn^{III}_{0.11}Mn^{IV}_{1.89}]O_4$	3.95	8.034(1)
	Relith.	$(Li_{0.89})[Mn^{III}_{0.89}Mn^{IV}_{1.11}]O_4$	3.56	8.194(5)
$x=0.1$	Delith.	$(Li_{0.18})[Co_{0.10}Mn^{III}_{0.08}Mn^{IV}_{1.82}]O_4$	3.90	8.042(3)
	Relith.	$(Li_{0.85})[Co_{0.10}Mn^{III}_{0.86}Mn^{IV}_{1.03}]O_4$	3.52	8.213(1)
$x=0.2$	Delith.	$(Li_{0.37})[Co_{0.21}Mn^{III}_{0.09}Mn^{IV}_{1.70}]O_4$	3.85	8.045(1)
	Relith.	$(Li_{0.88})[Co_{0.20}Mn^{III}_{0.74}Mn^{IV}_{1.06}]O_4$	3.53	8.203(1)
$x=0.5$	Delith.	$(Li_{0.52})[Co_{0.50}Mn^{III}_{0.02}Mn^{IV}_{1.48}]O_4$	3.73	8.053(1)
	Relith.	$(Li_{0.87})[Co_{0.50}Mn^{III}_{0.42}Mn^{IV}_{1.12}]O_4$	3.55	8.145(1)

[a]Assumes all cobalt is trivalent. ( ) and [ ] denote tetrahedral and octahedral site occupancy, respectively.

Table 4 EXAFS determined structural parameters for delithiated and relithiated $LiCo_xMn_{2-x}O_4$ (where $x=0.2$)

		M–O		M–M		
M	Sample	R^a/Å	σ/Å	R^a/Å	σ/Å	Residue (%)[b]
Mn	Parent	1.908	0.070	2.898	0.074	1.1
	Delithiated	1.905	0.053	2.856	0.059	2.6
	Relithiated	1.907	0.064	2.899	0.071	1.4
Co	Parent	1.929	0.056	2.877	0.067	2.8
	Delithiated	1.928	0.051	2.856	0.063	0.9
	Relithiated	1.931	0.057	2.881	0.066	3.1

[a]Uncertainties in distances (±0.01 Å) are estimated from the difference between EXAFS refined values and those obtained from X-ray diffraction in the reference compound $LiMn_2O_4$. [b]Residue $=\Sigma_k(k[\chi_{exp}(k)]-k[\chi_{calc}(k)])^2k^3/\Sigma_k(k[\chi_{exp}(k)]^2-k^3)$.

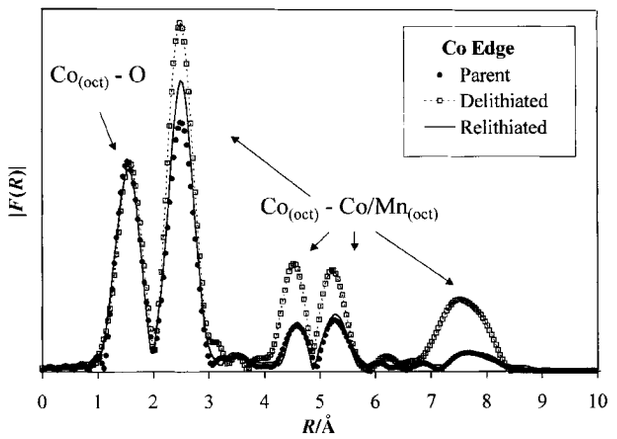

Fig. 6 Fourier transforms of the cobalt edge EXAFS of the parent $LiCo_{0.2}Mn_{1.8}O_4$, lithium extracted and lithium reinserted phases.

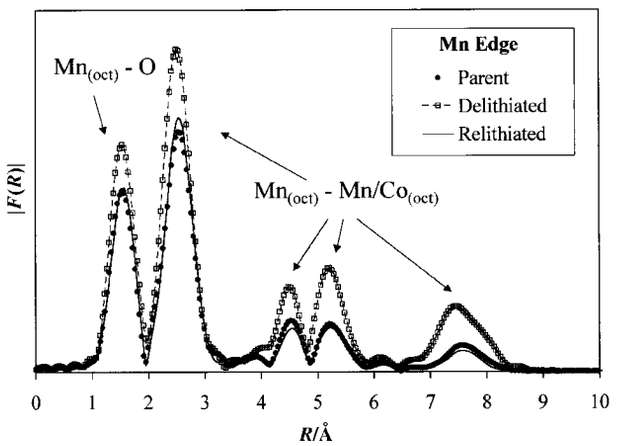

Fig. 7 Fourier transforms of the manganese edge EXAFS of the parent $LiCo_{0.2}Mn_{1.8}O_4$, lithium extracted and lithium reinserted phases.

Changes in the cobalt–metal distances and extent of local disorder mirror the changes in cell volume brought about by manganese oxidation. Similar to the parent compounds, the delithiated and relithiated phases also show a difference in the EXAFS derived R_{Mn-M} and R_{Co-M} interatomic distances. The relithiated phases are similar in composition to the parent and have similar average oxidation states. However, the delithiated phases contain primarily Mn^{4+} and thus the local contraction about Co^{3+} in the delithiated spinels appears to arise from lower Coulombic repulsion by the lower charged Co^{3+} species, rather than from size effects.

The recently reported electrochemical extraction of lithium from $LiCo_{0.5}Mn_{1.5}O_4$ showed that two potential plateaux are observed,[6] the first at *ca.* 4 V and the second at *ca.* 5 V. Our analyses of $LiCo_{0.5}Mn_{1.5}O_4$ show that cobalt is present as Co^{3+} and manganese as Mn^{3+} and Mn^{4+}. Thus, the plateau observed at 4 V almost certainly arises from the Mn^{3+}/Mn^{4+} redox couple, similar to that observed in the non-doped materials, and that at 5 V from the Co^{3+}/Co^{4+} redox couple. The mild oxidising conditions used in our work are not sufficient to oxidise Co^{3+}, which results in an approximately 1:1 relationship between the quantity of cobalt in $LiCo_xMn_{2-x}O_4$ and the amount of lithium that remains after chemical extraction in acid.

Conclusions

Trivalent cobalt is favourable as a dopant into $LiM_xMn_{2-x}O_4$ due to the similarity in size between Co^{3+} and Mn^{4+}. At low concentrations, dopant cobalt significantly increases crystallinity, which is most notable for low temperature preparations. XAFS confirms that cobalt is homogeneously distributed in the lattice and is responsible for an increase in local order. The observed reduction of the spinel lattice cell volume with cobalt doping arises from a local contraction of the manganese lattice about substituted Co^{3+} ions. The previously reported electrochemical extraction of lithium from $LiCo_{0.5}Mn_{1.5}O_4$ at greater than 5 V allows nearly all of the lithium to be extracted. It appears from this study that the complete electrochemical

extraction of lithium occurs initially by the oxidation of Mn^{3+} to Mn^{4+} followed by oxidation of Co^{3+} to Co^{4+}.

Acknowledgements

This work was performed under the auspices of the Programme International de Coopération Scientifique (PICS N° 538) of the Centre National de la Recherche Scientifique (CNRS), France, and the France–New Zealand Cultural and Scientific Agreement (Ministère des Affaires Étrangères, France). The CEA-CNRS-MENESR is thanked for access to the XAS facilities at LURE. P.A was financed by the Pôle Universitaire Européen de Montpellier et du Languedoc-Roussillon, France, and B.A. by a Postdoctoral Fellowship from FoRST (New Zealand).

References

1 L. Guohua, H. Ikuta, T. Uchida and M. Wakihara, *J. Electrochem. Soc.*, 1996, **143**, 178.
2 G. Pistoia, G. Wang and C. Wang, *Solid State Ionics*, 1992, **58**, 285.
3 J. M. Tarascon, E. Wang, F. K. Shokoohi, W. R. McKinnon and S. Colson, *J. Electrochem. Soc.*, 1991, **138**, 2859.
4 G. Pistoia, A. Antonini, R. Rosati, C. Bellitto and G. M. Ingo, *Chem. Mater.*, 1997, **9**, 1443.
5 P. B. Aitchison, B. Ammundsen, D. J. Jones, J. Rozière, B. Bonnet and G. R. Burns, Proc. MRS Spring Meeting 1999, San Francisco, USA, April 1999, in press.
6 H. Kawai, M. Nagata, H. Tukamoto and A. West, *J. Mater. Chem.*, 1998, **8**, 837.
7 B. Ammundsen, D. J. Jones, J. Rozière and F. Villain, *J. Phys. Chem. B*, 1998, **102**, 7939.
8 A. Yamada and M. Tanaka, *Mater. Res. Bull.*, 1995, **30**, 715.
9 *Collected Abstracts of Powder Diffraction Meeting, Toulouse*, 1990, p. 127.
10 M. J. Katz, R. C. Clarke and W. F. Nye, *Anal. Chem.*, 1956, **28**, 507.
11 A. Michalowicz, *Logiciels pour la Chimie*, Société Française de Chimie, Paris, 1991, p. 102.
12 S. I. Zabinsky, J. J. Rehr, A. Ankudinov, R. C. Albers and M. J. Eller, *Phys. Rev. B*, 1995, **52**, 2995.
13 B. Ammundsen, D. J. Jones, J. Rozière and G. R. Burns, *Chem. Mater.*, 1996, **8**, 2799.
14 S. Suzuki, M. Tomita, S. Okada and H. Arai, *J. Phys. Chem. Solids*, 1996, **57**, 1851.
15 M. M. Thackeray, A. de Kock and W. I. F. David, *Mater. Res. Bull.*, 1993, **28**, 1041.
16 'Occam's Razor', attributed to William of Occam, born 1285 (Surrey), died 1349 (Munich). See for example, J. Cohen and I. Stewart, *The collapse of chaos*, Viking Press, NY, 1994.
17 J. C. Hunter, *J. Solid State Chem.*, 1981, **39**, 142.
18 B. Ammundsen, D. J. Jones, J. Rozière and G. R. Burns, *Chem. Mater.*, 1995, **7**, 2151.
19 X. Shen and A. Clearfield, *J. Solid State Chem.*, 1986, **64**, 270.
20 K. Ooi, Y. Miyai and J. Sakakihara, *Langmuir*, 1991, **7**, 1167.
21 Q. Feng, Y. Miyai, H. Kanoh and K. Ooi, *Langmuir*, 1992, **8**, 1861.
22 B. Ammundsen, P. B. Aitchison, G. R. Burns, D. J. Jones and J. Rozière, *Solid State Ionics*, 1997, **97**, 269.

Paper 9/05784F